Available online at www.sciencedirect.com
SCIENCE DIRECT
Journal of Power Sources 157 (2006) 271–283
JOURNAL OF POWER SOURCES
www.elsevier.com/locate/jpowsour

A computational simulation of a hydrogen/chlorine single fuel cell

M. Thomassen[a,*], B. Børresen[a], K. Scott[b], R. Tunold[a]

[a] *Department of Materials Science and Engineering, Group of Electrochemistry, Norwegian University of Science and Technology, NO-7491 Trondheim, Norway*

[b] *School of Chemical Engineering and Advanced Materials, University of Newcastle upon Tyne, Newcastle upon Tyne NE1 7RU, UK*

Received 11 November 2004; received in revised form 7 July 2005; accepted 11 July 2005
Available online 29 August 2005

Abstract

A two-dimensional, isothermal mathematical model of an H_2–Cl_2 single fuel cell with an aqueous HCl electrolyte is presented. The model focuses on the electrode reactions in the chlorine cathode and also includes the mass and momentum balances for the electrolyte and cathode gas diffusion layer. There is good agreement between the model predictions and experimental results. Distributions of physical parameters such as reactant and product concentrations, solution and solid phase potentials and local current densities and overpotentials as a function of cell voltage are presented. Effects of varying the initial electrolyte concentration and operating pressure are analysed. It was found that an electrolyte inlet concentration of 6 mol dm^{-3} gave the best cell performance and that an increase of operating pressure gave a steady increase of the fuel cell performance.

Keywords: Hydrogen chlorine fuel cell; Mathematical modeling; Porous gas diffusion electrode; Hydrochloric acid

1. Introduction

Fuel cells are in general used as generators of electrical energy, either for mobile or stationary applications. In a H_2–Cl_2 fuel cell, oxygen is replaced by chlorine as the oxidizing agent; hence, the product from this cell is not water, but hydrogen chloride. Consequently, the H_2–Cl_2 fuel cell is as much an electrochemical reactor as a generator of electrical power. The use of H_2–Cl_2 fuel cells for co-production of hydrochloric acid and electrical power in industrial applications has been proposed for plants having an excess of hydrogen and chlorine readily available; the chlor-alkali industry has a potential for energy savings with the use of H_2–Cl_2 fuel cells [1]. The use of H_2–Cl_2 fuel cells in industrial processes where chlorine is produced as a by-product, for example, in magnesium electrolysis, can also be beneficial. H_2–Cl_2 fuel cells have also been proposed for space applications [2] and for distributed energy storage systems [3–5].

A mathematical model of a fuel cell provides a better understanding of the complex, coupled phenomena that occur in such systems, as well as useful information for scale-up and design. It also enables prediction of the cell performance as a function of operating conditions. To our knowledge, no mathematical models of H_2–Cl_2 fuel cells have previously been presented in the literature. However, the system has strong resemblances to the alkaline fuel cell, of which several models have been presented [6,7]. In addition, the system also has similarities with the PEM fuel cell which has been extensively modeled [8–17].

In this paper, a two-dimensional, *steady-state*, isothermal model for a single cell of a hydrogen chlorine fuel cell is presented. The model considers four of the six layers of the H_2–Cl_2 single cell: membrane, separator, cathode catalyst layer and the cathode gas diffusion layer. The mathematical model is solved using the Femlab 3.0a® program package and the chemical engineering toolbox from Comsol AB. Profiles of local overpotential, current density and electrolyte concentration are obtained as a function of cell voltage and electrolyte concentration.

* Corresponding author. Tel.: +47 73594040; fax: +47 73594083.
E-mail address: magnus.thomassen@material.ntnu.no (M. Thomassen).

0378-7753/$ – see front matter © 2005 Elsevier B.V. All rights reserved.
doi:10.1016/j.jpowsour.2005.07.034

Nomenclature

a^{g}	specific area of the gas–electrolyte interface ($cm^2\ cm^{-3}$)
a_i^{A}	activity of species i, adsorbed on electrode surface
a_i^{b}	activity of species i, in bulk solution
A_{cat}	catalyst surface area ($cm^2\ g^{-1}$)
c_e	electrolyte concentration ($mol\ cm^{-3}$)
c_g	molar concentration of an ideal gas at a specific temperature and 1 bar (4.036×10^5 at 25°C) ($mol\ cm^{-3}\ bar^{-1}$)
c_i	concentration of species i ($mol\ cm^{-3}$)
c_i^0	concentration of species i at a reference condition ($mol\ cm^{-3}$)
d_{cat}	electrode catalyst loading ($mg\ cm^{-2}$)
D_i	free stream diffusivity of species i ($cm^{-2}\ s^{-1}$)
$D_i'^{g}$	effective gas diffusivity of species i ($cm^{-2}\ s^{-1}$)
$D_i'^{l}$	effective liquid phase diffusivity of species i ($cm^{-2}\ s^{-1}$)
E^{rev}	theoretical open circuit potential at the given conditions (V)
E^0	theoretical open circuit potential at standard conditions (V)
F	Faraday's constant ($96485.309\ C\ mol^{-1}$)
H_i	Henry's law constant for species i ($mol\ cm^{-3}\ bar^{-1}$)
i	local current density ($A\ cm^{-2}$)
i_0	exchange current density ($A\ cm^{-2}$)
I	total current density of single cell ($A\ cm^{-2}$)
L_i	length of layer i (cm)
m_i	reaction order of species i
M_i	symbol for the chemical formula of species i
n	number of electrons transferred
$\mathbf{N}_i$	molar flux of species i ($mol\ cm^{-2}\ s^{-1}$)
p_i	partial pressure of species i (bar)
p_i^{v}	vapour pressure of species i (bar)
Q_{ox}	quantity of charge to reduce surface oxide ($mC\ cm^{-2}$ and $\mu C\ cm^{-2}$)
R	ideal gas constant ($8.31451\ J\ K^{-1}\ mol^{-1}$)
R_i^{e}	electrochemical reaction rate per unit volume species i ($mol\ cm^{-3}\ s^{-1}$)
R_i^{p}	mass transfer rate over phase boundary species i ($mol\ cm^{-3}\ s^{-1}$)
s_i	stoichiometric coefficient of species i
t	time (s)
T	absolute temperature (K)
u_i	free stream mobility of species i ($mol\ cm^2\ J^{-1}\ s^{-1}$)
u_i'	effective mobility of species i ($mol\ cm^2\ J^{-1}\ s^{-1}$)
U	electrical potential of an electronically conductive solid phase (V)
U_{cell}	cell voltage (V)
$\mathbf{v}$	volume average velocity ($cm\ s^{-1}$)
V_{cat}	specific catalyst volume (cm)
z_i	charge number of species i

Greek letters

α_a	anodic transfer coefficient
α_c	cathodic transfer coefficient
δ	thickness of electrolyte film (cm)
ϵ	porosity
η	local overpotential (V)
κ_c	electronic conductivity of cathode ($S\ cm^{-1}$)
κ_m	ionic conductivity of membrane ($S\ cm^{-1}$)
ξ	dimensionless spatial coordinate
Φ	solution phase potential (V)

Superscripts

e	electrochemical reaction
g	gas phase
l	liquid phase
p	mass transport across phase boundary
v	vapour pressure
0	reference condition

Subscripts

(ads)	adsorbed specie
(aq)	solvated
AN	anode
c	cathode
cat	catalyst (RuO_2)
CCL	cathode catalyst layer
DIFF	cathode diffusion layer
i	species i
j	species j
(l)	liquid phase
m	membrane
MEM	membrane
SEP	separator
+	cations (H^+)
−	anions (Cl^-)

2. Description of system

The H_2–Cl_2–FC single cell considered in this study consists of six layers: an anode gas diffusion layer, an anode catalyst layer, a Nafion® 117 membrane, a separator layer, a cathode catalyst layer and a cathode gas diffusion layer. A schematic diagram of the cell is shown in Fig. 1. The anode is a conventional PEMFC-electrode, based either on a carbon cloth or carbon paper, with a thin layer of Pt/C electrocatalyst bonded to a Nafion® 117 membrane. The separator layer consists of a porous polyphenylene sulphide (PPS) cloth and a circulating hydrochloric acid electrolyte. The cathode is con-

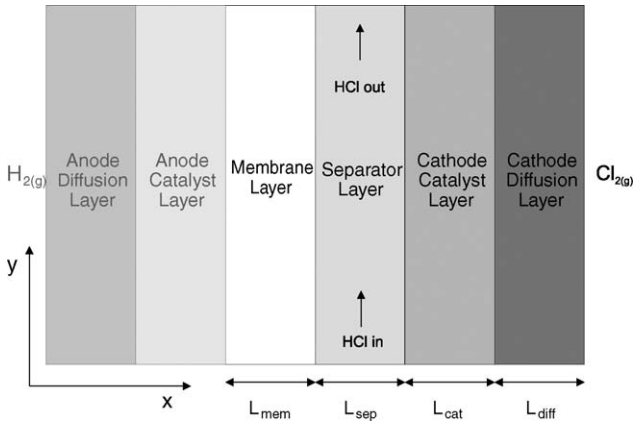

Fig. 1. Schematic diagram of the H_2–Cl_2–FC single cell.

structed of a highly Teflon-impregnated carbon paper acting as the gas diffusion layer and a thin, porous catalytic layer consisting of RuO_2 particles.

The most distinct feature of the H_2–Cl_2 fuel cell is the cathode catalyst layer and the separator (electrolyte) layer. To simplify the model, the anode gas diffusion and catalyst layers are considered to play a negligible role in the overall performance of the cell, due to the rapid oxidation kinetics and high diffusivity of hydrogen, and are thus omitted from the mathematical model. The presence of the liquid electrolyte and its intimate contact with the Nafion membrane will probably ensure a higher degree of membrane humidification than normally found in PEM-fuel cells. Thus, the Nafion® 117 membrane is considered to be fully humidified and acting as an ideal proton conductor with a constant conductivity. In addition, as a consequence of the forced convection of the liquid electrolyte, a rapid mass transport within is to be expected. It is therefore assumed that the mass transfer of the electrolyte and its dissolved species across the membrane layer is negligible and that the membrane thus acts as an impermeable barrier. The gaseous chlorine supplied to the cathode gas chamber diffuses across the cathode gas diffusion layer and the catalyst layer through macropores in the electrode. The chlorine then dissolves in the electrolyte in the catalyst layer, diffuses through the electrolyte film covering the catalyst particles and reacts electrochemically on the catalyst surface according to the following reaction:

$$Cl_{2(aq)} + 2e^- \rightleftharpoons 2Cl^- \tag{1}$$

The electrons needed by the above reaction move from the current collector, across the gas diffusion and catalyst layers where they are consumed by the chlorine reduction reaction. The product, chloride ions, either diffuses through the micropores into the bulk electrolyte (separator layer) or recombines with protons in the electrolyte and evaporates as gaseous HCl and diffuses through the gas diffusion layer and into the gas channels. Each layer of the cell is assumed to be a superposition of two or more continua. This assumption is based on the porous electrode model presented by Newman and Thomas-Alyea [18]. It is also assumed that in the gas diffusion electrode, the micropores are occupied only by the liquid phase and the macropores only by the gas phase.

3. Mathematical modeling

3.1. Governing equations

The equation of continuity for species i in a porous medium can be written in the general form:

$$\frac{\partial \epsilon c_i}{\partial t} = -\nabla \mathbf{N}_i + R_i^{\mathrm{e}} + R_i^{\mathrm{p}} \tag{2}$$

where ϵ is porosity, t the time, c_i and $\mathbf{N}_i$ refer to the concentration and molar flux of species i, respectively, and R_i^{e} and R_i^{p} indicate the electrochemical reaction rate and mass transfer rate of species i per unit volume of the electrode.

3.2. The flux expression

The flux expression, $\mathbf{N}_i$, depends on whether the species exists in the gas or liquid phase. It is assumed that only chlorine and hydrogen chloride exist in the gas phase and that these species have an ideal gas behaviour. Thus, Fick's law for binary diffusion can be used

$$\mathbf{N}_i^{\mathrm{g}} = -D_i'^{\mathrm{g}} c_{\mathrm{g}} \nabla p_i \tag{3}$$

where $D_i'^{\mathrm{g}}$ is the effective gas diffusivity, c_{g} the molar concentration of an ideal gas at the current temperature and 1 bar and p^i is the partial pressure of species i. For the liquid phase, it is assumed that the flux equation for dilute solutions can be employed:

$$\mathbf{N}_i^{\mathrm{l}} = -D_i'^{\mathrm{l}} \nabla c_i - z_i u_i' F c_i \nabla \Phi + c_i \mathbf{v} \tag{4}$$

where F is Faraday's constant, Φ the solution phase potential, v the volume average velocity and $D_i'^{\mathrm{l}}$, z_i and u_i' are the effective liquid phase diffusivity, charge number and effective mobility of species i, respectively.

The effective diffusivity and mobility is corrected for porosity and tortuosity by applying the Bruggemann correction [18]:

$$D_i' = D_i \epsilon^{1.5} \tag{5}$$

$$u_i' = u_i \epsilon^{1.5} \tag{6}$$

where D_i and u_i are the free stream diffusivity and mobility of species i.

3.2.1. Interfacial mass transfer

With the assumption of equilibrium at the gas–electrolyte interface, the mass transport rate, R_i^{p}, for species i across a phase boundary can be approximated to:

$$R_i^{\mathrm{p}} = -a^{\mathrm{g}} D_i^{\mathrm{l}} \left(\frac{H_i p_i - c_i}{\delta} \right) \tag{7}$$

where a^{g} is the specific area of the gas–electrolyte interface, H_i the Henry's law constant of species i and δ is the thickness of the electrolyte film.

3.2.2. Electrochemical reaction rate

The electrochemical reaction rate of species i per unit volume, R_i^{e}, can be represented by:

$$R_i^{e} = -\frac{s_i a^{l} i}{nF} \tag{8}$$

where a^{l} is the specific area of the catalyst–electrolyte interface, n denotes the number of electrons transferred while i is the local current density and s_i is the stoichiometric coefficient of species i.

The stoichiometric coefficient is given by expressing an electrochemical reaction in the form:

$$\sum_i s_i M_i^{z_i} \rightarrow n e^{-} \tag{9}$$

where M_i is a symbol for the chemical formula of species i.

The local current density, i, can be described by the Butler–Volmer equation:

$$i = i_0 \left[\prod_i \left(\frac{c_i}{c_i^0} \right)^{m_i} \exp\left(\frac{\alpha_a n F \eta}{RT} \right) - \prod_j \left(\frac{c_j}{c_j^0} \right)^{m_j} \exp\left(\frac{-\alpha_c n F \eta}{RT} \right) \right] \tag{10}$$

where i_0 is the exchange current density, c_i^0 and m_i correspond to the concentration of species i at a reference condition and the reaction order of species i and α_a and α_c denote the apparent anodic and cathodic transfer coefficients, respectively.

The local overpotential, η, is given by:

$$\eta = U - \Phi - E^{rev} \tag{11}$$

where U is the electrical potential of an electronically conductive solid phase and E^{rev} is the reversible electrode potential at the given concentrations given by:

$$E^{rev} = E^0 - \frac{RT}{nF} \sum_i s_i \ln\left(\frac{c_i}{c_i^0} \right) \tag{12}$$

where E^0 is the theoretical open circuit potential at standard conditions.

3.2.3. Electroneutrality

In the liquid phase, the distribution of the charged species must obey the electroneutrality condition:

$$\sum_i z_i c_i = 0 \tag{13}$$

3.3. Membrane layer

There are no electrochemical reactions in this layer and there are no gas, liquid or electronic conductive phases present. It is assumed that the potential drop in this layer can be described by Ohm's law.

$$\nabla \Phi_{mem} = \frac{I}{\kappa_m} \tag{14}$$

where I is the total current of the single cell and κ_m is the conductivity of the membrane. Since there are no electrochemical reactions occurring in this layer, the current density is constant. By differentiating Eq. (14), the potential drop in the membrane can be expressed as:

$$\nabla^2 \Phi_{mem} = 0 \tag{15}$$

3.4. Separator (electrolyte) layer

There are no electrochemical reactions in this layer and there are no gas phase or electrically conductive solid phase present. Four species exist in this layer: liquid water, dissolved chlorine and two ions— $H^{+}_{(aq)}$ and $Cl^{-}_{(aq)}$. By employing the continuity equation and the transport equations to all species, except water, one obtains:

$$\nabla(D'_+ \nabla c_+) + \nabla\left(\frac{z_+ D'_+ F}{RT} c_+ \nabla \Phi \right) - \nabla(c_+ \mathbf{v}) = 0 \tag{16}$$

$$\nabla(D'_- \nabla c_-) + \nabla\left(\frac{z_- D'_- F}{RT} c_- \nabla \Phi \right) - \nabla(c_- \mathbf{v}) = 0 \tag{17}$$

$$\nabla(D'_{Cl_2} \nabla c_{Cl_2}) - \nabla(c_{Cl_2} \mathbf{v}) = 0 \tag{18}$$

Since there are no reactions or mass transfers over phase boundaries in this layer, there is no change in the volume average velocity (neglecting the influence of the density change due to HCl dissolution):

$$\nabla \mathbf{v} = 0 \tag{19}$$

Due to the porous PPS cloth, which the electrolyte has to flow through, it is assumed that the electrolyte flow in the y-direction can be described by a plug flow characteristic.

3.5. Catalyst layer

Assuming that there are no electrochemical reactions in the gas phase of the catalyst layer, gaseous chlorine dissolves into the electrolyte before reacting. The product, HCl, either diffuses into the bulk electrolyte or evaporates into the gas phase and diffuses to the gas channels. Because of the low vapour pressure of water at 25 °C, it is assumed that there is negligible amounts of water vapour in the gas phase; thus, the transport equation for chlorine gas becomes:

$$N_{Cl_2} = -D'_{Cl_2} c_g \nabla p_{Cl_2} \tag{20}$$

and the following equation can be obtained from the continuity equation:

$$\nabla(D'^{g}_{Cl_2} c_g \nabla p_{Cl_2}) - a_c^g D'^{g}_{Cl_2} \left(\frac{H_{Cl_2} p_{Cl_2} - c_{Cl_2}}{\delta_c} \right) = 0 \quad (21)$$

In the liquid phase, the mass transport of the dissolved reactant gases can be written by using the Nernst–Planck equation (Eq. (4)). Since the dissolved chlorine gas is an electrically neutral species, the second term on the right-hand side is zero. The dissolved gas reacts electrochemically at the catalyst–electrolyte interface; thus, the following equation is obtained at steady state:

$$\nabla(D'^{l}_{Cl_2} \nabla c_{Cl_2}) - \nabla(c_{Cl_2}\mathbf{v}) + a_c^g D'^{g}_{Cl_2} \left(\frac{H_{Cl_2} p_{Cl_2} - c_{Cl_2}}{\delta_c} \right) - \frac{s_{Cl_2} a_c^l i_c}{n_c F} = 0 \quad (22)$$

The local current density at the cathode, i_c, is described by applying the Butler–Volmer equation to the chlorine reduction reaction:

$$i_c = i_{0,c} \left[\left(\frac{c_-}{c_-^0} \right)^{m_-} \exp\left(\frac{\alpha_a F \eta_c}{RT} \right) - \left(\frac{c_{Cl_2}}{c^0_{Cl_2}} \right)^{m_{Cl_2}} \exp\left(\frac{-\alpha_c F \eta_c}{RT} \right) \right] \quad (23)$$

The transport equation for gaseous hydrochloric acid becomes:

$$N_{HCl} = -D'_{HCl} c_g \nabla p_{HCl} \quad (24)$$

Thus, with the interfacial mass transport rate of HCl being:

$$R^p_{HCl} = -a_c^g D'^{g}_{HCl} c_g \left(\frac{p^v_{HCl} - p_{HCl}}{\delta_c} \right) \quad (25)$$

where p^v_{HCl} is the concentration dependent vapour pressure of HCl, the following equation can be obtained from the continuity equation:

$$\nabla(D'^{g}_{HCl} c_g \nabla p_{HCl}) + a_c^g D'^{g}_{HCl} c_g \left(\frac{p^v_{HCl} - p_{HCl}}{\delta_c} \right) = 0 \quad (26)$$

Protons do not react electrochemically at the cathode, while the electrochemical reaction rate for chloride ions follows Eq. (8). Thus, using the continuity, flux and Butler–Volmer equations, we get:

$$\nabla(D'^{l}_{+} \nabla c_+) + z_+ F \nabla(u_+ c_+ \nabla \Phi) - \nabla(c_+ \mathbf{v}) - a_c^g D'^{g}_{HCl} c_g \left(\frac{p^v_{HCl} - p_{HCl}}{\delta_c} \right) = 0 \quad (27)$$

$$\nabla \left(D'^{l}_{-} \nabla c_- \right) + z_- F \nabla(u_- c_- \nabla \Phi) - \nabla(c_- \mathbf{v}) - \frac{s_- a_c^l i_c}{n_c F} - a_c^g D'^{g}_{HCl} c_g \left(\frac{p^v_{HCl} - p_{HCl}}{\delta_c} \right) = 0 \quad (28)$$

The total current density, I, obtained from the single cell must be equal to the integrated value of the local current density, i, with respect to the thickness (x) of the cathode catalyst layer:

$$I = -\int_0^{L_{cat}} a^l i \, dz \quad (29)$$

As for the membrane layer, Ohm's law can describe the potential drop in the solid catalyst particles. Differentiating Eq. (29) and combining it with Ohm's law gives the following expression for the potential drop in the cathode catalyst layer:

$$\nabla^2 U = \frac{a_c^l i_c}{\kappa_c} \quad (30)$$

where κ_c is the effective electrical conductivity of the cathode.

3.6. Gas diffusion layer

There are no electrochemical reactions in this layer; gaseous chlorine diffuses from the gas channels towards the catalyst layer while the product, HCl, diffuses from the catalyst layer towards the gas channels. As for the catalyst layer, it is assumed that no water vapour exists in the gas phase. The transport equation for chlorine gas and gaseous hydrochloric acid becomes:

$$N_i = -D'_i c_g \nabla p_i \quad (31)$$

As for the catalyst layer, the potential drop can be described by Ohm's law:

$$\nabla U = \frac{I}{\kappa_d} \quad (32)$$

where κ_d is the effective conductivity of the diffusion layer. Since no electrochemical reactions occur in the gas diffusion layer, I is constant. By differentiating Eq. (32), the potential drop in the layer can be expressed as:

$$\nabla^2 U_{diff} = 0 \quad (33)$$

3.7. Boundary conditions

3.7.1. Anode/membrane interface

At this interface, only protons are transferred and the flux of protons must be equal to the total current density:

$$N_+|_{SEP} = \frac{I}{nF} \quad (34)$$

Since the anode has been omitted from this model, the electrical potential at the anode/membrane interface can be arbi-

trarily fixed. Hence, the membrane potential at this boundary is set to zero:

$$\Phi_{\text{mem}}|_{\text{AN}} = 0 \tag{35}$$

3.7.2. Membrane/separator interface

The membrane acts as an impermeable barrier for the electrolyte and its dissolved species. Thus, the fluxes of anions and chlorine are zero, while the flux of protons is continuous at this interface

$$\mathbf{N}_{\text{Cl}_{2(\text{aq})}}|_{\text{SEP}} = 0 \tag{36}$$

$$\mathbf{N}_{-}|_{\text{SEP}} = 0 \tag{37}$$

$$\mathbf{N}_{+}|_{\text{MEM}} = \mathbf{N}_{+}|_{\text{SEP}} \tag{38}$$

The solution potential is equal to the membrane potential.

$$\Phi_{\text{mem}}|_{\text{MEM}} = \Phi_{\text{sep}}|_{\text{SEP}} \tag{39}$$

3.7.3. Separator/cathode catalyst interface

It is assumed that the PPS-separator prevents gaseous reactants from flowing towards the opposite electrode. Thus, the fluxes of gaseous chlorine and hydrochloric acid are zero at this interface:

$$\mathbf{N}_{i(\text{g})}|_{\text{CCL}} = 0 \Rightarrow \nabla p_i|_{\text{CCL}} = 0 \tag{40}$$

Since the separator is an electronic insulator, the electronic current density in this layer is zero:

$$\nabla U|_{\text{CCL}} = 0 \tag{41}$$

The fluxes of dissolved chlorine and ions are continuous at this interface:

$$\mathbf{N}_{+}|_{\text{CCL}} = \mathbf{N}_{+}|_{\text{SEP}} \tag{42}$$

$$\mathbf{N}_{-}|_{\text{CCL}} = \mathbf{N}_{-}|_{\text{SEP}} \tag{43}$$

$$\mathbf{N}_{\text{Cl}_{2(\text{aq})}}|_{\text{CCL}} = \mathbf{N}_{\text{Cl}_{2(\text{aq})}}|_{\text{SEP}} \tag{44}$$

3.7.4. Cathode catalyst/gas diffusion layer interface

Since the gas diffusion layer prevents leakage of electrolyte, it is assumed that the fluxes of the electrolyte and its dissolved species are zero at this boundary. The fluxes of chlorine gas and gaseous hydrochloric acid are continuous at this boundary.

$$\mathbf{N}_{i(\text{g})}|_{\text{DIFF}} = \mathbf{N}_{i(\text{g})}|_{\text{CCL}} \tag{45}$$

$$\mathbf{N}_{+}|_{\text{DIFF}} = 0 \tag{46}$$

$$\mathbf{N}_{-}|_{\text{DIFF}} = 0 \tag{47}$$

$$\mathbf{N}_{\text{Cl}_{2(\text{aq})}}|_{\text{DIFF}} = 0 \tag{48}$$

3.7.5. Gas diffusion layer/gas channel interface

The electrical potential can be arbitrarily fixed either at the anode or cathode current collector. Setting the value of the anode to zero, U_c at this interface will be:

$$U_{\text{c}} = U_{\text{cell}} \tag{49}$$

where U_{cell} is the total cell voltage.

Assuming a uniform distribution of gases in the gas channels, the partial pressure of chlorine and hydrochloric acid can be set to:

$$p_{\text{Cl}_2} = p^0_{\text{Cl}_2} \tag{50}$$

$$p_{\text{HCl}} = 0 \tag{51}$$

3.7.6. Electrolyte inlet

At $y = 0$, the electrolyte concentration and volume average velocity are known. It is also assumed that the chlorine concentration in the supplied electrolyte is equal to 1% of the saturation amount since the electrolyte is recycled and removal of all chlorine gas from this electrolyte is difficult.

$$c_{\text{e}}|_{y=0} = c^0_{\text{e}} \tag{52}$$

$$\mathbf{v}_x|_{y=0} = \mathbf{v}^0_x \tag{53}$$

$$c_{\text{Cl}_2}|_{y=0} = 0.01 \cdot c_{\text{Cl}_2,\text{sat}} \tag{54}$$

3.7.7. Electrolyte outlet

At $y = 1$, the change in electrolyte and chlorine concentration is zero. It is assumed that the mass transport due to diffusion and migration is negligible compared to the convective flux.

$$\nabla(c_{\text{e}}|_{y=1}) = 0 \tag{55}$$

$$\nabla(c_{\text{Cl}_{2(\text{aq})}}|_{y=1}) = 0 \tag{56}$$

$$\nabla(\mathbf{v}_y|_{y=1}) = 0 \tag{57}$$

4. Model parameters and correlation

Using realistic values for the modeling parameters is essential for the viability of the mathematical model. A reasonable choice of the parameter values is thus as important as the mathematical modeling itself. Hence, an effort has been made to supply as realistic values as possible for these parameters.

4.1. Thermodynamic properties

4.1.1. Solubility of chlorine

It is assumed that the solubility of chlorine gas obeys Henry's law:

$$c_i = H_i p_i \tag{58}$$

The solubility of chlorine changes linearly with the hydrochloric acid concentration in the range applicable for this model. Using the data from [19], the following correlation was obtained for the solubility of chlorine in hydrochloric acid at 25 °C:

$$H_{\text{Cl}_2}(c_{\text{H}^+}) = 0.0077 \cdot c_{\text{H}^+} + 6.0 \times 10^{-5} \tag{59}$$

4.1.2. Vapour pressure of HCl

The vapour pressure of HCl over hydrochloric acid increases exponentially with increasing hydrochloric acid concentration. At 25 °C, the following correlation was obtained using the data from *Perry's Chemical Engineers' Handbook* [20]:

$$p^{v}_{HCl}(c_{H^+}) = 2.4 \times 10^{-6} \exp(961.46 \cdot c_{H^+}) \quad (60)$$

4.1.3. Transport properties

The mobility of the electrolyte species changes with electrolyte concentration. Using the data in [21], the following correlations were obtained:

$$u_{Cl^-} = 7 \times 10^{-9} \exp(-171.51 \cdot c_e) \quad (61)$$

$$u_{H^+} = 4 \times 10^{-8} \exp(-171.51 \cdot c_e) \quad (62)$$

The diffusivities of the charged species were found using the Nernst–Einstein equation:

$$D_i = RTu_i \quad (63)$$

The diffusion coefficient for chlorine is assumed not to be influenced by the acid concentration. The diffusion coefficient in 0.1N HCl at 25 °C has been found to be 1.38×10^{-5} cm^2 s^{-1} [22]. The electrical conductivities of the catalyst and gas diffusion layers are reported to be 7.14 S cm^{-1} [23] and 12.5 S cm^{-1}, respectively. Earlier work from our group [24] investigated the conductivity of Nafion® 117 and found a value of 0.1 S cm^{-1} at 25 °C in a 0.3 mol dm^{-3} HCl solution.

4.1.4. Kinetic parameters

The exchange current density, i_0, for chlorine reduction on RuO_2 has been measured to be $\sim 1.0 \times 10^{-5}$ in 1 mol dm^{-3} HCl saturated with Cl_2 using the rotating disc electrode technique [25]. The anodic and cathodic Tafel slopes for the chlorine evolution/reduction reaction on RuO_2 have been reported by several authors to be 40 and 120 mV dec^{-1}, respectively [26,27]. Thus, the anodic and cathodic transfer coefficients, α_a and α_c, are 0.75 and 0.25, respectively. Since the electrochemical reactions within the cathode catalyst layer are considered to be elementary reactions, the same absolute values as the stoichiometric coefficients are used as reaction orders of the reactants and products. The electrochemical kinetic parameters are listed in Table 1.

Table 1
Electrochemical kinetic parameters

Parameter	Value
Number of electrons transferred, n	2
Stoichiometric coefficient of chlorine, s_{Cl_2}	−1
Stoichiometric coefficient of chloride, s_{Cl^-}	2
Reaction order of chlorine, m_{Cl_2}	1
Reaction order of chloride, m_{Cl^-}	2
Anodic transfer coefficient, α_a	0.75
Cathodic transfer coefficient, α_c	0.25
Exchange current density, i_0 (A cm^{-2})	1.0×10^{-5}

4.1.5. Structural parameters

The thickness of the cathode catalyst layer was found to be 10 μm by analysing a cross-section of an electrode in a scanning electron microscope. The gas diffusion electrode, Toray carbon paper had a thickness of 0.4 mm. The specific surface area of the RuO_2 catalyst was 45–65 m^2 g^{-1} (Alpha Aesar) and the catalyst loading was 2 mg cm^{-2}. By assuming perfect wetting of the whole catalyst surface, the specific catalyst–electrode interface area, a^l, can be calculated from:

$$a^l = \frac{d_{cat}}{V_{cat}} \cdot A_{cat} \quad (64)$$

where d_{cat} is the catalyst loading (g cm^{-2}), V_{cat} the specific catalyst volume (cm) and A_{cat} is the catalyst surface area (cm^2 g^{-1}).

Hence, the value of a^l in the cathode catalyst layer has a value of 9×10^5 cm^2 cm^{-3}. Several researchers have reported specific gas–electrolyte interface areas of the order of 10^3 cm^2 cm^{-3} and an electrolyte film thickness of ~0.5 μm [21,28]. Thus, the values for a^g and δ have been set to 1.0×10^3 and 0.5 μm, respectively. The structural parameters are listed in Table 2.

4.1.6. Operating conditions

The operating conditions for the laboratory test cell are ambient temperature and pressure. The base case operating conditions for the model are listed in Table 3.

4.2. Method of solution

The model equations are highly coupled and non-linear and a numerical solution is required. The finite element method program Femlab® 3.0a with the chemical engineer-

Table 2
Base case structural parameters

Parameter (unit)	Membrane layer	Separator layer	Catalyst layer	Gas diffusion layer
Layer thickness, L_i (cm)	0.0175	0.08	1.0×10^{-3}	0.04
Gas phase porosity, ϵ^g			0.1	0.7
Liquid phase porosity, ϵ^l		0.5	0.3	
Solid phase porosity, ϵ^s			0.6	0.3
Specific area of gas–electrolyte interface, a^g (cm^{-1})			1.0×10^3	
Specific area of catalyst–electrolyte interface, a^l (cm^{-1})			1.0×10^5	
Thickness of electrolyte film, δ (cm)			5.0×10^{-4}	
Electrical conductivity (S cm^{-1})	0.10		7.14	12.5

Table 3
Base case operating conditions

Parameter (unit)	Value
Electrolyte inlet concentration, C_e (mol cm^{-3})	0.003
Operating temperature, T (°C)	25
Operating pressure, p^0 (bar)	1
Electrolyte flow rate, $\mathbf{v}$ (cm s^{-1})	0.02

ing toolbox from Comsol AB was employed to solve the equations. A multiphysics model incorporating three application modes and six dependent variables was created and a weak, non-linear parametric solver was used to solve the constructed model.

5. Experimental validation

The experimental single cell is a further development of a cell examined in [29]. Fig. 2 shows a schematic illustration of the fuel cell construction. The housing consisted of two graphite current collectors with double serpentine flow fields, a carbon paper anode attached to a Nafion 117 membrane, a polyphenylene sulphide (PPS) cloth separator, a carbon paper cathode and a silicon gasket. The graphite current collectors included inlets and outlets for the circulating liquid HCl electrolyte. The PPS cloth acts as a spacer between the electrodes making it possible to apply a mechanical pressure to the electrodes and simultaneously supplying space for the circulating electrolyte.

5.1. Cathode preparation

The cathodes were constructed of ELAT carbon paper (E-TEK) with various amounts of Teflon impregnation (0–60 wt%). Catalyst inks were prepared using commercial unsupported RuO_2 catalyst (Alpha Aesar). The catalyst was mixed with various amounts of Teflon suspension and isopropanol to produce a range of catalysts with different degrees of wet-proofing. The mixture was stirred and ultrasonicated for several hours before application to the cathode carbon paper electrode using an air-brush (Badger), with the carbon electrode placed on a thermal-controlled heating plate. After spraying, the electrode was dried in a forced convection oven at 150 °C for 1 h.

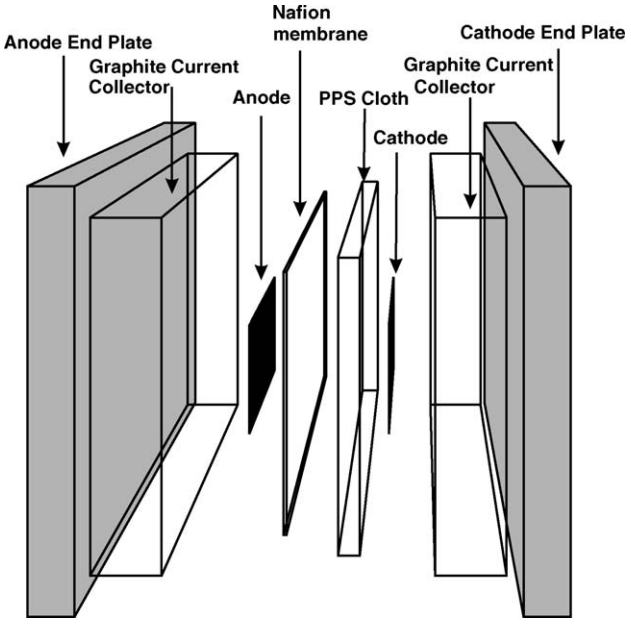

Fig. 2. Schematic illustration of the hybrid fuel cell construction.

5.2. Membrane and MEA preparation

The Nafion 117 membranes were treated by immersion in 85 °C 18.2 MΩ distilled water for 15 min, thereafter in 5% H_2O_2 (Merck p.a.) for 30 min and washed with distilled water and ion exchanged twice in 0.05 M H_2SO_4 (Merck p.a.), each time for 30 min. After ion exchange, the membranes were washed thoroughly by immersion in distilled water four times, each for about 15 min. The membranes were then cut in rectangular pieces and stored in purified water. Commercially available ELAT gas diffusion electrodes (E-TEK) with a 20 wt% Pt/C catalyst loading of 1 mg Pt cm^{-2} were used as anodes. A rectangular piece of Nafion membrane was gently dried with a lint free paper, sandwiched with a 6.5 cm^2 rectangular anode piece between two thin Teflon sheets and hot-pressed for 3 min at 130 °C and 10 MPa. The MEA was then cooled down and placed in purified water until mounted in the cell.

5.3. Fuel cell testing

The cell was assembled using a torque of 0.15 N m on the bolts. All experiments reported here were conducted at room temperature and atmospheric pressure. The gases, hydrogen (5.0 AGA) and chlorine (2.8 Gerling Holtz), were fed to the cell without any kind of pre-heating or humidification and exited the cell through a water column to create a small overpressure inside the cell (10 cm H_2O). The fuel cell was controlled using a Solartron SI1287 electrochemical interface. Quasi-steady-state polarization curves were recorded at an operating temperature of 25 °C by sweeping the potential at 1 mV s^{-1} from open circuit to approximately 0.2 V and then reversed. The HCl liquid electrolyte circulated from a thermally controlled external reservoir through the cell at a rate of 0.2 ml s^{-1} via a peristaltic pump. The HCl electrolyte concentration was 3 mol dm^{-3}.

6. Results and discussion

The model developed is a two-dimensional model and the fuel cell performance and the distribution of the physical parameters will vary along the cell length (y-axis). It was found that, for the base case electrolyte velocity, this variation was negligible from a distance of 0.05 cm from the electrolyte

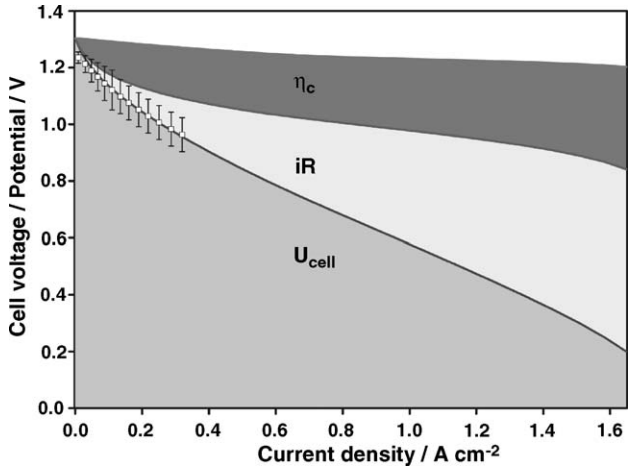

Fig. 3. Polarization curve for base case. The open squares are experimental results from a 6 cm^2 laboratory cell. The cathodic overpotential (η_c) and *iR* drop of the cell are also shown.

inlet for all current densities. The results presented in this section are taken from a point 0.5 cm from the electrolyte inlet and are considered to give a good representation of the distribution of the physical parameters inside the whole cell.

6.1. Comparison of model with experimental results

A comparison of the model prediction for the base case with experimental data obtained with the laboratory test cell described above is presented in Fig. 3. The open squares represent the mean values from five experimental runs with error bars giving the corresponding deviation from the mean values, while the full line is the model prediction. The relatively large uncertainty in the experimental results is due to a very unstable operation and low experimental reproducibility of the laboratory cell. The experimental aspects of this cell will be discussed in more detail in an upcoming paper. Furthermore, no experimental results were recorded above 0.35 A cm^{-2} due the potentiostat limiting current range of 2 A.

6.2. Polarization curve for base case

The polarization curve for the base case presented in Fig. 3 displays a typical shape for low temperature fuel cells. It includes two of the three distinguishable zones: activation controlled, ohmic controlled and mass transport controlled polarization. The activation controlled zone is much less pronounced than in similar polarization curves for H_2–O_2 fuel cells. This is most probably because the kinetics of chlorine reduction is faster than the kinetics for oxygen reduction; the exchange current density for chlorine reduction on ruthenium oxide is $\sim 1.0 \times 10^{-5}$ A cm^{-2}, compared to the exchange current density of oxygen reduction on platinum, which has a value of $\sim 1.0 \times 10^{-9}$ A cm^{-2} [30]. The slope of the linear region corresponds to a cell resistance of approximately 0.56 Ω cm^2. The fuel cell has an open circuit voltage of 1.26 V and at a cell voltage of 0.2 V, no limiting current can be observed. Although a slight increase of the slope of the polarization curve can be seen. The maximum power density of the cell is about 0.58 W cm^{-2} at a cell voltage of 0.55 V (determined from the mathematical model). The *iR* drop in the membrane and electrolyte and the cathodic overpotential predicted by the mathematical model are also shown in Fig. 3. The overpotential dominates the losses at low current densities, while at current densities above 0.6 A cm^{-2}, the *iR* drop is responsible for more than 50% of the polarization losses. At very high current densities (>1.6 A cm^{-2}), the cathode overvoltage starts to increase more rapidly, indicating an impending mass transport controlled limiting current.

6.3. Distribution of physical variables

The distribution of the partial pressure of gaseous chlorine as a function of cell voltage and dimensionless spatial coordinate, ξ, is given in Fig. 4. It can be seen that with decreasing cell voltage, the distribution of the partial pressure of chlorine becomes less uniform. At a cell voltage of 0.2 V, the partial pressure of chlorine inside the catalyst layer is approximately 0.85 atm with a small gradient towards the diffusion layer. This indicates that even though there exists a certain mass transfer resistance for the chlorine gas, it is not the factor limiting the total cell performance. The distribution of dissolved chlorine is shown in Fig. 5. At cell voltages between 1.2 and 0.9 V, there is only a very slight decrease of the chlorine concentration. With a further lowering of the cell voltage, an interesting phenomenon occurs: the concentration of dissolved chlorine increases and reaches a peak value at $U_{cell} \approx 0.75$ V. Below 0.75 V, the chlorine concentration rapidly decreases. This unexpected behaviour is due to the increasing solubility of chlorine with increasing electrolyte concentration (see Fig. 6 and Eq. (59)). At 0.75 V, the electrolyte concentration reaches a plateau value and low-

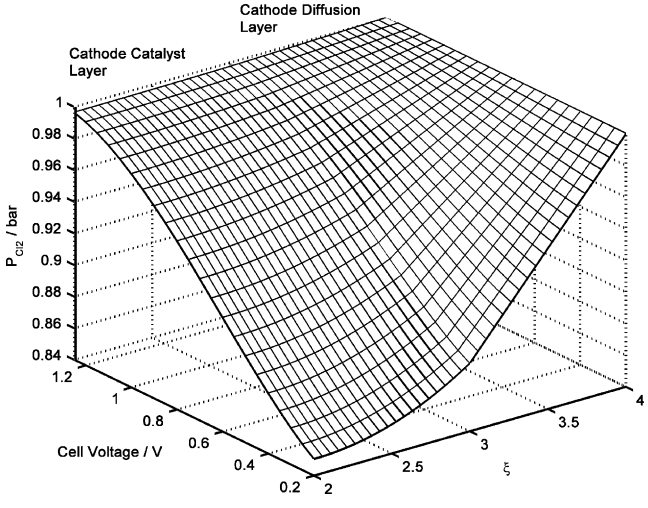

Fig. 4. Chlorine partial pressure distribution in the cathode catalyst and diffusion layer as a function of cell voltage.

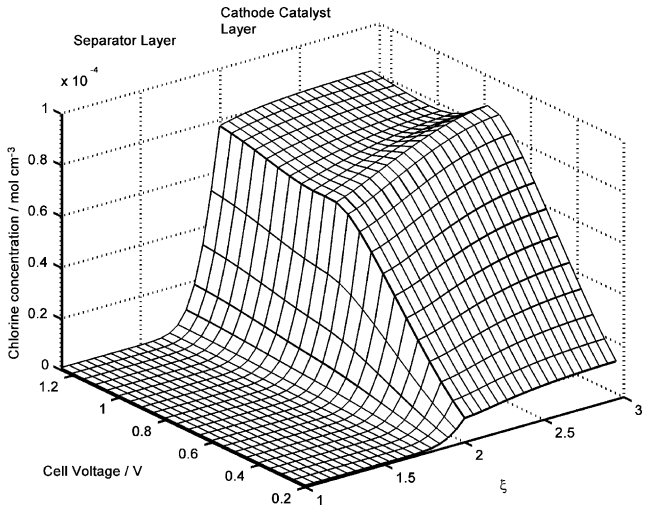

Fig. 5. Dissolved chlorine concentration distribution in electrolyte and cathode catalyst layers as a function of cell voltage.

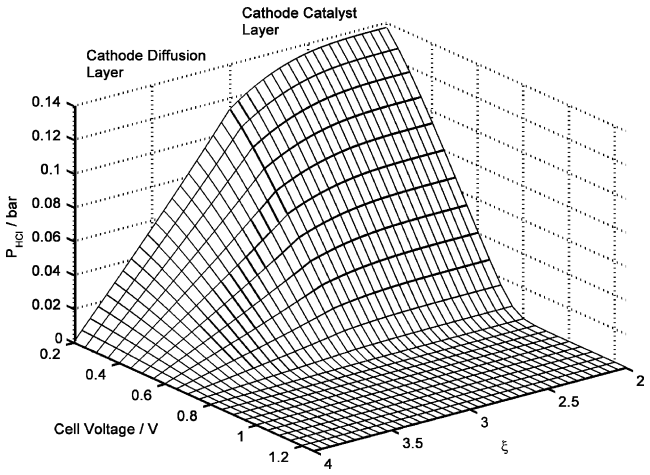

Fig. 7. HCl partial pressure distribution in the cathode catalyst and diffusion layer as a function of cell voltage.

ering the cell voltage further increases the electrochemical reduction rate of the chlorine reduction reaction and the concentration of dissolved chlorine drops. The low concentration of dissolved chlorine at low cell voltages indicates that this parameter is the cause of the tendency of a limiting current behaviour observed in Fig. 3. Fig. 6 displays the concentration distribution of HCl in the electrolyte as a function of cell voltage. It can be seen that there is a drastic increase in acid concentration with decreasing cell voltage down to 0.6 V where it reaches a plateau value. This increase is caused by the production of chloride ions from the reduction of chlorine and the diffusional and migrational fluxes of chloride ions are too low to maintain a concentration close to the inlet concentration. This high electrolyte concentration inside the catalyst layer has several effects: it causes a drop in the reversible voltage of the cathodic reaction and exposes the cathode catalyst to a more corrosive environment. Another effect, not taken into consideration in this work, is the possibility of increased adsorption of Cl^- with increasing HCl concentration which may reduce the chlorine reduction rate. The electrolyte has a maximum conductivity at concentrations close to 5 mol dm^{-3}; thus, the concentration build-up inside the catalyst layer has a negative effect on the conductivity in this layer, causing a higher ohmic drop.

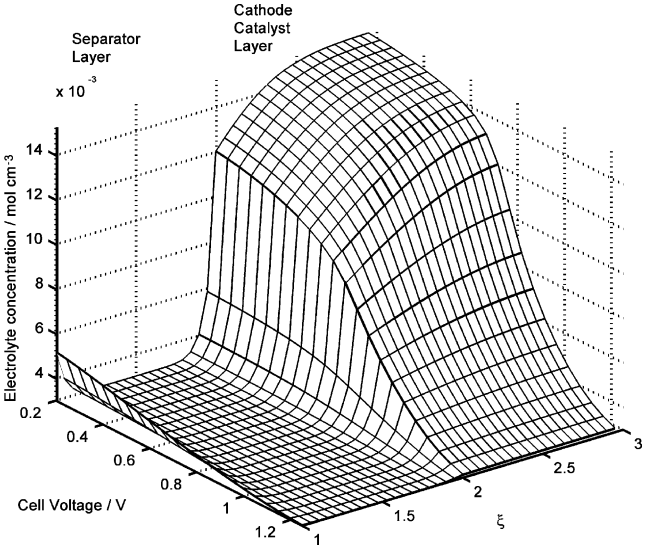

Fig. 6. Electrolyte concentration distribution in the electrolyte and cathode layer as a function of cell voltage.

On the other hand, a positive effect of the concentration increase is a higher solubility of chlorine in the catalyst layer. Fig. 7 shows the distribution of the partial pressure of gaseous HCl in the catalyst and diffusion layers as a function of cell voltage. The evaporation of HCl has a strong correlation with the concentration of hydrochloric acid in the catalyst layer shown in Fig. 6. This phenomenon manifests itself only at low cell voltages, where the partial pressure of hydrochloric acid reaches values of approximately 0.15 atm. It does not seem that the mass transport resistance of gaseous hydrochloric acid out of the catalyst layer has any major effect on the cell performance. Figs. 8 and 9 show the profiles of the local apparent current density and local overvoltage, respectively. The distribution of these parameters is very uniform through the catalytic layer at all cell voltages, it is only at low cell voltages that a small curvature close to the separator layer can be seen on the local current density distribution. The local overvoltage of the cathode reaches a value of −0.36 V at a cell voltage of 0.2 V and does not have the typical Tafelian behaviour. This is probably due to the increasing electrolyte concentration and the depletion of dissolved chlorine in the catalyst layer at low cell voltages, which effectively increases the overvoltage value additionally. Fig. 10 shows the profile of the membrane and solution potentials as a function of cell voltage. The variation across the membrane and separator layers corresponds to the ohmic drop between the electrodes. The potential drop in the cathode catalyst layer is negligible compared to the quite large drops in the separator and membrane layers. The figure also shows that although the

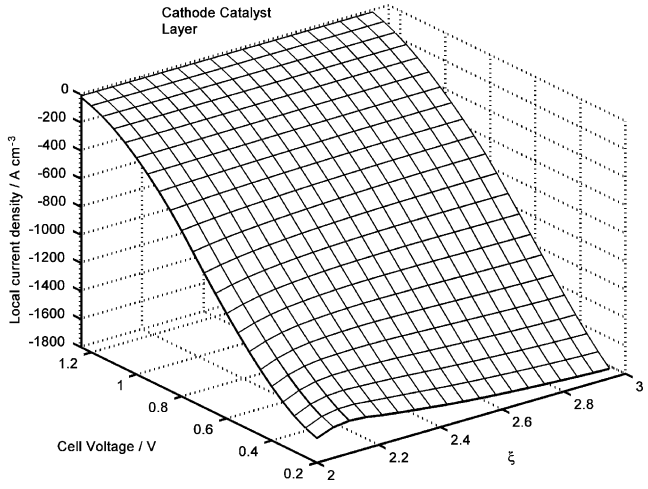

Fig. 8. Profile of the local current density in the cathode layer as a function of cell voltage.

separator layer is almost five times thicker than the membrane layer, the potential drop across the two layers is nearly equal.

6.4. Influence of operating conditions

6.4.1. Initial electrolyte concentration

Since most thermodynamic, transport and kinetic parameters are influenced by the electrolyte concentration, a variation of the initial electrolyte concentration can have a strong effect on the cell performance. For instance, increasing the electrolyte concentration will increase the solubility of chlorine, but above 5 mol dm^{-3}, the conductivity will decrease. In addition, an increase of the chloride concentration will affect the cathode kinetics by increasing the influence of the anodic back reaction and reducing the theoretical open circuit voltage, E_{rev}.

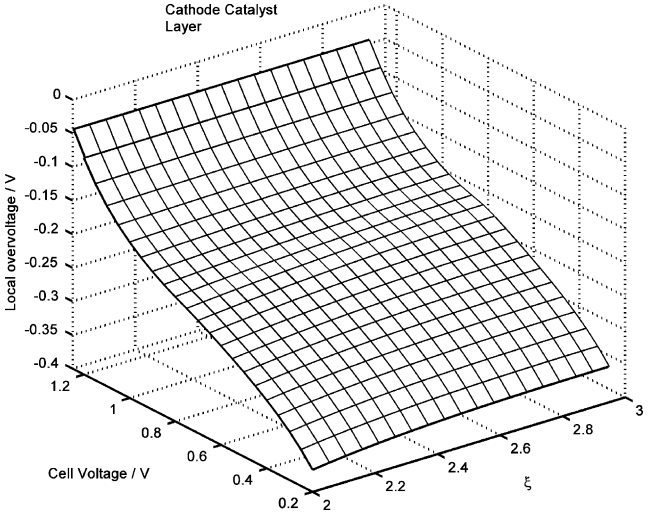

Fig. 9. Profile of the local overvoltage in the cathode layer as a function of cell voltage.

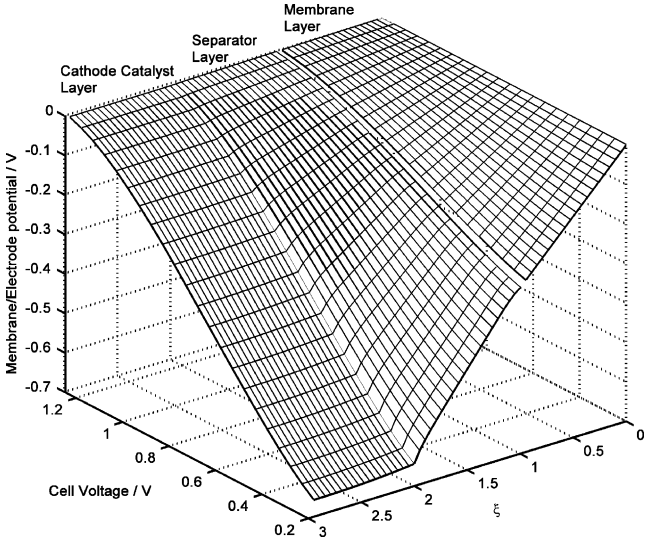

Fig. 10. Profile of the membrane and solution potentials as a function of cell voltage.

Polarization curves for a single cell with different electrolyte inlet concentrations are given in Fig. 11. A considerable increase in the cell performance can be seen when increasing the electrolyte concentration from 1 to 3 mol dm^{-3} and as expected, the open circuit voltage drops somewhat. A further increase from 3 to 5 mol dm^{-3} has an negligible effect. This behaviour was observed previously on a fuel cell similar to the experimental cell presented in this work [29]. In Fig. 12, the effect of initial electrolyte concentration on current density as a function of cell voltage is presented. At high cell voltage, the variation of electrolyte inlet concentration has a very low effect on the total current density of the cell. At lower cell voltages, the current density increases significantly with increasing concentration from 1 to 3 mol dm^{-3} and moves through a broad maximum at concentrations around 6 mol dm^{-3}. The dashed line in Fig. 12 shows the conductivity of hydrochloric acid as a function of concentration. It is clear that although the current density concentration dependence has the same trend as the electrolyte conductivity, the effect is not as pronounced. This indicates that other mechanisms, such as electrode kinetics and mass transport, influence the electrolyte concentration dependence of the current density.

6.4.2. Operating pressure

Polarization curves for the single cell at different operating pressures are presented in Fig. 13. An increase in the cell current density at all voltages can be observed, while the polarization curves maintain essentially the same slope in the ohmic polarization region. The small tendency towards limiting current behaviour observed at an operating pressure of 1 bar is completely eliminated at higher pressures. The reason for the increased cell performance is a higher interfacial mass transport of chlorine from the gas phase to the liquid phase and a higher solubility of chlorine in the electrolyte.

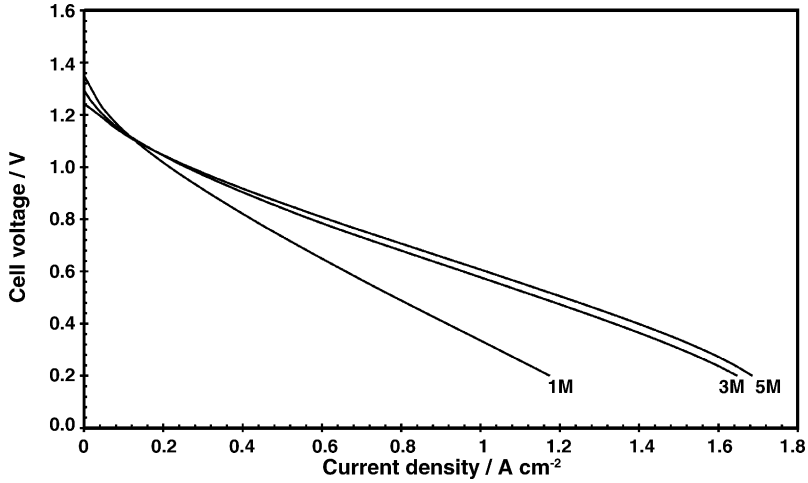

Fig. 11. Single cell polarization curves at different electrolyte inlet concentrations.

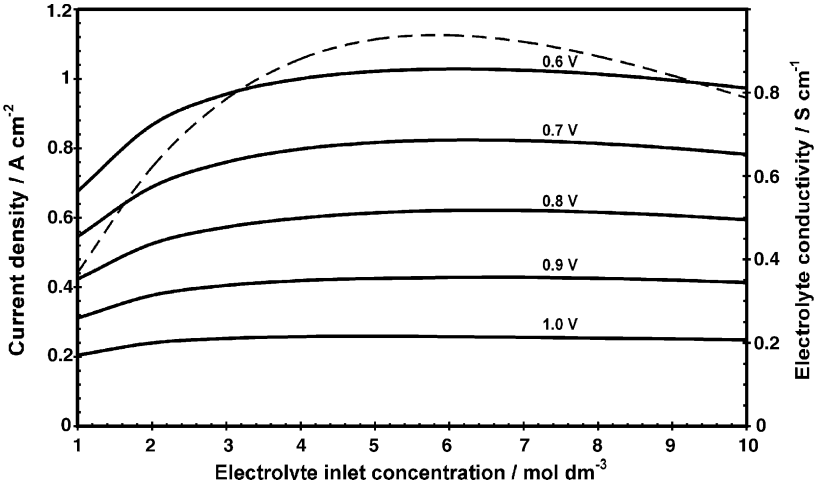

Fig. 12. Cell current density as a function of electrolyte inlet concentration and cell voltage. Dashed line represents the conductivity of HCl as a function of electrolyte concentration.

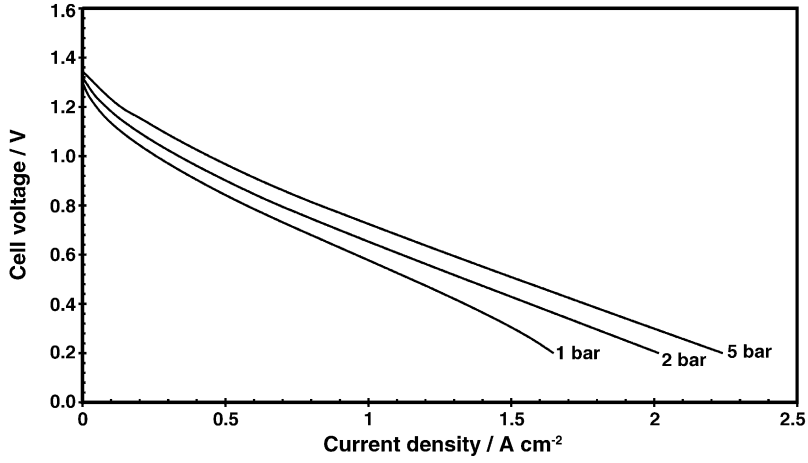

Fig. 13. Single cell polarization curves at different operating pressures.

There is no indication that the conductivity of the electrolyte varies with the operating pressure.

7. Conclusions

A mathematical model for a H_2–Cl_2 single fuel cell has been developed. The model describes mass transport and electrochemical reactions occurring in the cathode gas diffusion layer, the cathode catalyst layer and the separator/membrane layers. From the profiles of dissolved chlorine as a function of cell voltage, it is determined that the interfacial mass transport of chlorine between the gas and liquid phases in the cathode probably is the rate-determining step at high current densities. It is found that concentration of the HCl electrolyte inside the cathode catalyst layer approaches values close to that of concentrated hydrochloric acid (12 mol dm^{-3}), especially at high current densities.

Influences of the operating condition of the fuel cell are investigated. It is shown that the cell performance increases substantially by increasing the inlet concentration of the hydrochloric acid electrolyte from 1 to 3 mol dm^{-3}. Increasing the electrolyte concentration further only leads to small changes in the overall cell performance. By increasing the operating pressure, a steady increase of the cell performance due to faster electrode kinetics can be observed.

Acknowledgements

The authors gratefully acknowledge the financial support of the Norwegian Research Council (NFR) and Norsk Hydro ASA. Research was supported by the FP5 Marie Curie HOST Fellowship Contract no. HPMT-CT-2001-00333.

References

[1] E. Anderson, E.J. Taylor, N.R.K. Vilambi, A. Gelb, Sep. Sci. Technol. 25 (1990) 1537.
[2] E.B. Anderson, E.J. Taylor, G. Wilemski, A. Gelb, J. Power Sources 47 (1994) 321–328.
[3] D.T. Chin, R.S. Yeo, J. McBreen, S. Srinivasan, J. Electrochem. Soc. 126 (1979) 713.
[4] R.S. Yeo, J. McBreen, S. Srinivasan, J. Electrochem. Soc. 126 (1979) C379.
[5] R.S. Yeo, J. McBreen, A.C.C. Tseung, S. Srinivasan, J. Mcelroy, J. Appl. Electrochem. 10 (1980) 393.
[6] J.H. Jo, S.C. Yi, J. Power Sources 84 (1999) 87–106.
[7] J.H. Jo, S.K. Moon, S.C. Yi, J. Appl. Electrochem. 30 (2000) 1023–1031.
[8] D.M. Bernadi, M.W. Verbrugge, AIChE J. 37 (1991) 1151–1163.
[9] D.M. Bernadi, M.W. Verbrugge, J. Electrochem. Soc. 139 (1992) 2477–2491.
[10] T. Berning, N. Djilali, J. Electrochem. Soc. 150 (2003) A1589–A1598.
[11] T. Berning, N. Djilali, J. Power Sources 124 (2003) 440–452.
[12] T. Berning, D.M. Lu, N. Djilali, J. Power Sources 106 (2002) 284–294.
[13] M. Ceraolo, C. Miulli, A. Pozio, J. Power Sources 113 (2003) 131–144.
[14] P.T. Nguyen, T. Berning, N. Djilali, J. Power Sources 130 (2004) 149–157.
[15] T.E. Springer, T.A. Zawodzinski, M.S. Wilson, S. Gottesfeld, J. Electrochem. Soc. 143 (1996) 587–599.
[16] T.E. Springer, M.S. Wilson, S. Gottesfeld, J. Electrochem. Soc. 140 (1993) 3513–3526.
[17] T.E. Springer, T.A. Zawodzinski, S. Gottesfeld, J. Electrochem. Soc. 138 (1991) 2334–2342.
[18] J. Newman, K.E. Thomas-Alyea, Electrochemical Systems, John Wiley & Sons, Hoboken, NJ, 2004.
[19] K.J. Vetter, in: A.S. Kertes, J.W. Lorimer (Eds.), Chlorine Solubilities in IUPAC Solubility Data Series, vol. 12, Pergamon Press, Oxford, 1983.
[20] R.H. Perry, D.W. Green, J.O. Maloney, Perry's Chemical Engineers' Handbook, vol. 7, McGraw Hill, New York, 1997.
[21] Q.F. Li, G. Xiao, H.A. Hjuler, R.W. Berg, N.J. Bjerrum, J. Electrochem. Soc. 141 (1994) 3114–3119.
[22] A. Tang, O.C. Sandall, J. Chem. Eng. Data 30 (1985) 189–191.
[23] K. Lasch, G. Hayn, L. Jorissen, J. Garche, O. Besenhardt, J. Power Sources 105 (2002) 305–310.
[24] R. Halseid, P.J.S. Vie, R. Tunold, J. Electrochem. Soc. 151 (2004) A381–A388.
[25] M. Thomassen, B. Børresen, G. Hagen, R. Tunold, Electrochim. Acta 50 (2005) 1157–1167.
[26] L.I. Krishtalik, Electrochim. Acta 26 (1981) 329–337.
[27] S. Trasatti, G. Lodi, in: S. Trasatti (Ed.), Electrodes of Conductive Metal Oxides, Part B, Elsevier, Amsterdam, 1981.
[28] T. Kenjo, J. Electrochem. Soc. 133 (1986) 2051–2058.
[29] M. Thomassen, B. Bøorresen, G. Hagen, R. Tunold, J. Appl. Electrochem. 33 (2003) 9–13.
[30] A. Damjanovic, J.O. Bockris, Electrochim. Acta 11 (1966) 376–377.